

Article

A Multi-Scale Approach in Hydraulic Characterization of a Metamorphic Aquifer: What Can Be Inferred about the Groundwater Abstraction Possibilities

Antonella Baiocchi ¹, Walter Dragoni ², Francesca Lotti ¹, Simone M. Piacentini ² and Vincenzo Piscopo ^{1,*}

¹ Department of Ecological and Biological Sciences, University of Tuscia, Viterbo 01100, Italy; E-Mails: baiocchi@unitus.it (A.B.); f.lotti@unitus.it (F.L.)

² Department of Physics and Geology, University of Perugia, Perugia 06100, Italy; E-Mails: dragoni@unipg.it (W.D.); piacentinism@libero.it (S.M.P.)

* Author to whom correspondence should be addressed; E-Mail: piscopo@unitus.it; Tel.: +39-0761-357-743; Fax: +39-0761-357-751.

Academic Editor: David Kreamer

Received: 10 July 2015 / Accepted: 20 August 2015 / Published: 27 August 2015

Abstract: Hard-rock aquifers, which constitute a water supply source in many countries, are highly heterogeneous and defining a realistic model of an aquifer can be extremely complex. The objective of this study was to hydraulically characterize a metamorphic aquifer in a representative area of Italy and to identify the most appropriate approach for tapping of groundwater in this challenging environment. The results of surface fracture surveys, injection tests, pumping tests, and a simplified numerical model were compared. From the surface fracture survey, a model of the rock mass characterized by a well-developed discontinuity network and by a high frequency of discontinuities resulted. The injection tests showed the extreme heterogeneity and the lower hydraulic conductivity of the rock mass in comparison with the results of the pumping tests. The independent estimate of the hydraulic parameter resulting from numerical model highlighted a range of values higher than those resulting from the pumping tests. The study demonstrated that the continuum medium approach can be used in the case of hard-rock aquifers with a dense network of discontinuities. The multi-scale approach is recommended for investigating hydraulic heterogeneity and significantly helps to identify the most promising areas for well locations and their characteristics in relation to the style of fracturing.

Keywords: hard-rock aquifers; hydraulic properties; aquifer heterogeneity; numerical modeling; Italy

1. Introduction

Hard-rock aquifers constitute a water supply source in many regions of Africa, America, and Asia. These aquifers are generally characterized by a low yield due to their low intrinsic primary permeability and porosity. Several factors influence the occurrence of groundwater in hard rocks, such as lithology, geomorphology, tectonics, and climate conditions.

Many studies have shown that hard-rock aquifers are comprised of weathered mantle and fissured bedrock where the groundwater movement takes place. The hydraulic conductivity and storage of the weathered mantle and underlying fissured bedrock are derived from geodynamic and geomorphic processes. The fissures have been explained by several processes, such as lithostatic decompression, tectonic activity, cooling stress, and weathering processes. These two layers make up a composite aquifer followed in depth by the fresh basement, which is only locally permeable where tectonic fractures are present [1–8].

Hard-rock aquifers, such as those constituted by plutonic and metamorphic rocks, are recognized to be highly heterogeneous, particularly in relation to the different degrees of fracturing. This implies that the bedrock transmissivity can vary over many orders of magnitude [3,7,9–13]. Therefore, well yields are highly variable, and a high incidence of well failure occurs. Thus, defining a sustainable pumping rate is more difficult here than in other cases because of the extremely complex aquifer behavior. In this case, more so than in other cases, considerations of the discontinuous flow system, anisotropy, and heterogeneity are required to develop a reasonable model of the aquifer.

To plan for the optimal management and sustainable groundwater development of these aquifers when the bedrock is densely fractured, the continuum approach is the characterization method frequently used. This approach is less expensive than discrete-fracture or hybrid approaches. Even if several studies have concluded that the porous medium approximation is valid in densely fractured aquifers [14–16], the scientific debate is still open, particularly with regard to the scale at which the approximation becomes appropriate [17–22].

In Italy, where hard rocks outcrop over large areas in the Alps, Calabria, and Sardinia, the hydrogeological properties of plutonic and metamorphic rocks are not well known. The groundwater yields of these aquifers (generally less than 5×10^{-3} m³/s per km²) are lower than those in the more common carbonate and alluvial aquifers (up to 3×10^{-2} m³/s per km²), which are widely used for the water supply. The interest in hard-rock aquifers is, thus, generally scarce; nevertheless, the large extent of these rocks and the scarcity of water resources in Sardinia (where hard-rock aquifers constitute 51% of the regional area) and Calabria regions (where hard-rock aquifers constitute 39% of the regional area) justify a thorough analysis [23]. Interest in these aquifers becomes even more relevant in the framework of the ongoing climate change: most of the scenarios regarding future climate scenarios in the Mediterranean area suggest a reduction in rainfall and, thus, a reduction in water resources [24,25].

This is the context of our study, which concerns a dam site in metamorphic rock in southern Sardinia. The dam site provides an opportunity to characterize a hydraulically fractured, metamorphic aquifer using a multi-scale approach. The results of the surface fracture surveys, injection tests, pumping tests, and simplified numerical model were compared to examine the heterogeneity of the hard-rock aquifer and to verify the degree of approximation of the porous medium approach. The objective of the study was to hydrogeologically characterize these low-permeability rocks and to examine which approach could better represent the fractured aquifer. This is a key point in the identification of the appropriate tapping method in a hydrogeological environment where water resources are generally scarce, but are fundamental to the drinking and irrigation water supply.

2. Study Area

The area under examination is 25 km west of the town of Cagliari, in the Sardinia region (Figure 1), where the Paleozoic basement related to the Hercynian orogenic evolution outcrops. The Paleozoic basement consists of an originally-sedimentary succession (Lower Cambrian to Early Carboniferous) that was deformed during the Carboniferous period under the low metamorphic to anchizonal setting [26]. The Arburese Unit outcropping at the dam site consists of the Arenarie di San Vito Formation (Middle Cambrian to Lower Ordovician), which is several hundred meters thick and is composed of decimetric to metric alternations between micaceous metasandstones, quartzites, and metasilstones. Clastic, poorly-cemented sediments, from gravels to sands and silts, of the Upper Pleistocene to the Holocene overlay the metamorphic basement [27]. The structural framework is mainly linked to the Hercynian Orogeny and Pliocene tectonic events. The Hercynian tectonics favored the thrust of the Arburese Unit over the Upper Ordovician to Lower Carboniferous succession and its deformation in large scale folding with axes of folds E–W and N–S oriented. The Pliocene tectonics shallow modified the structural setting through normal fault systems E–W, and N–S to NNW–SSE oriented [28,29].

The hydrogeological properties of the Paleozoic basement are not well known. It is only known that metamorphic rocks form a low-permeability aquifer (until 20 years ago, these rocks were considered to be impervious) where groundwater circulation occurs in the fissured zones close to the surface (on average, the first tens of meters). In the most heavily fractured zones (*i.e.*, near the faults), the groundwater flow is more active and can occur at a greater depth [30].

The study site corresponds to the building zone of the Medau Zirimilis Dam (Figure 1), a 50-m-high rockfill dam that was completed with an upstream impervious face and with a grout curtain 10–50 m deep. The drainage basin of the reservoir, 29.5 km² of extension, is characterized by a typical Mediterranean climate with mean annual precipitation between 700 and 900 mm and air temperature between 15 and 16 °C.

During the construction of the dam and the initial reservoir filling, several hydrogeological investigations were conducted. One of these was the measurement of the seepage through the rock foundation and laterally to the dam, that discharged in the drainage systems located at the base of the dam embankment and downstream of the grout curtain. These and other investigations highlighted the fact that the groundwater circulation involved the most fissured layers closest to the surface, including,

on average, the first 50 m of the Paleozoic rocks, up to a depth of 100 m in the faulted zones. The most evident faulted zone has been found in the valley bottom at the site of the dam [30].

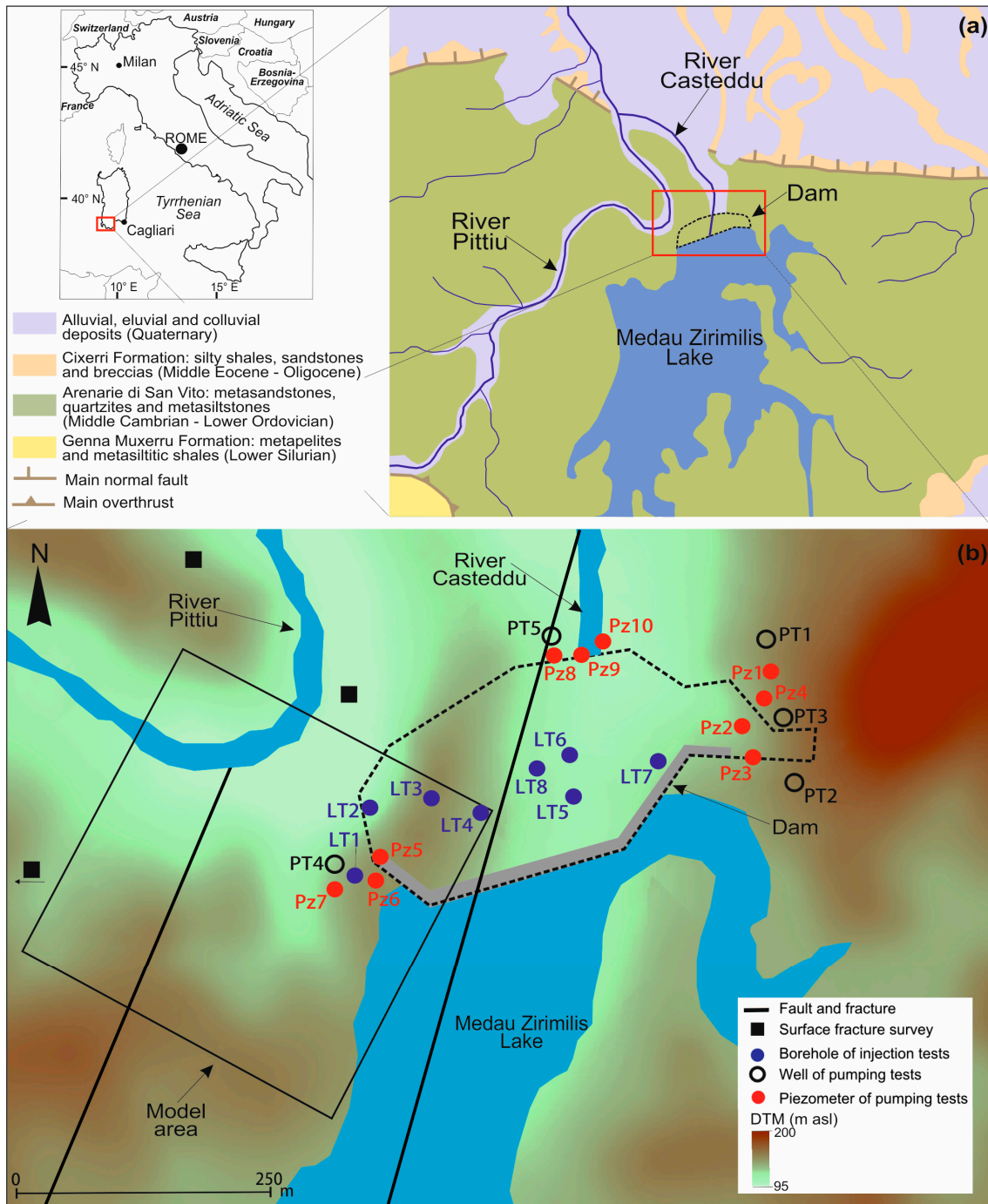


Figure 1. (a) Location of the study area; (b) Location of the surface fracture surveys, injection tests and pumping tests at the site of the Medau Zirimilis Dam.

3. Investigations, Materials, and Methods

The results of the previous surveys [30] have been revised, integrated and appropriately processed to obtain the hydraulic characterization of the Palaeozoic rocks. The field investigations at the dam site included a surface fracture survey, injection tests and pumping tests (Figure 1).

The surface fracture survey concerned the Arenarie di San Vito Formation on three rock walls (ranging in size from 20 to 30 m²) with different orientations located in the western sector of the dam (Figure 1): there were two vertical planes oriented to 60° N and 350° N and one horizontal plane. For each planar surface, the discontinuity orientation, the apparent aperture (measured by a feeler gauge with minimum determinable aperture of 0.05 mm), and the spacing between the discontinuities belonging to the same set were determined. The discontinuities considered were those having a trace length greater than 80% of the size of the measured plane (from 2 × 10 to 3 × 10 m).

The injection tests (Lugeon tests) concerned single-hole tests conducted on sealed sections with packers (from 3 to 5 m in length). Five pressure steps were applied (generally 0.2–0.5–1.0–0.5–0.2 MPa at the manometer), measuring the undisturbed water level before injection and making sure that the injected discharge was stabilized. A total of 76 tests were performed in eight boreholes penetrating the Arenarie di San Vito Formation (Figure 1) to a maximum depth of 60 m; one of the boreholes was drilled with a dip angle of 60° (LT8 in Figure 1).

During the initial reservoir filling, pumping tests were performed at five wells (Figure 1), with depths between 73 and 100 m (dip angle from 10° to 30°). The pumping tests lasted between 7.5 and 45 h at a constant rate between 2.1×10^{-3} and 3.5×10^{-3} m³/s, with the observation of a drawdown in at least one piezometer nearby the tested well. The pumping data were interpreted using analytical techniques [31] and commercial software (Aquifer Test 4.1, Nova Metrix GM, Kitchener, Canada).

Based on the results of the hydraulic characterization of the site, a simplified numerical model was constructed for the western sector of the dam site (Figure 1), where one of the tested wells is located, and nearby the outcrops of the surface fracture surveys. The purpose of the numerical simulation was to examine the results of pumping tests to a further scale, different from that of the analytical solutions and of the other hydraulic tests. The model was implemented with the code MODFLOW-2000 (Groundwater Vistas 6 graphical user interface). The reconstruction of the DTM provided the top elevation. The initial heads were obtained using the interpolation of the heads measured during the initial reservoir filling.

4. Results

The results are reported with reference to different methods of the hydraulic characterization and to the numerical simulation.

4.1. Discontinuity-Network Characterization

Two discontinuity types were identified in the examined outcrops. The first type consisted of regular bedding planes that were continuous at the scale of the outcrops and delimited the various metasandstone and metasilstone beds. The second type of discontinuity consisted of sub-vertical straight joints of varying orientations that cut the bedding planes.

The projection of the discontinuity poles on a stereographic net [32,33] made it possible to group the systematic discontinuities into three different sets (Figure 2). Table 1 lists the average values of the dip direction, dip angle and Fisher dispersion coefficient of each set.

The measured spacing approaches a log-normal distribution for the three sets. The apertures were measured on discontinuity segments when they were not altered by the weathering phenomena and

ranged from <0.05 mm (instrumental measurement limit) to 1 mm. None of the different distributions tested (normal, log-normal, logistic, gamma, and Weibull) perfectly represented the measured data. The log-normal distribution best represented the majority of the data, even if it contained a greater dispersion for the minimum and maximum values of the parameter. The statistics regarding the discontinuity spacing and the apparent aperture are listed in Table 1.

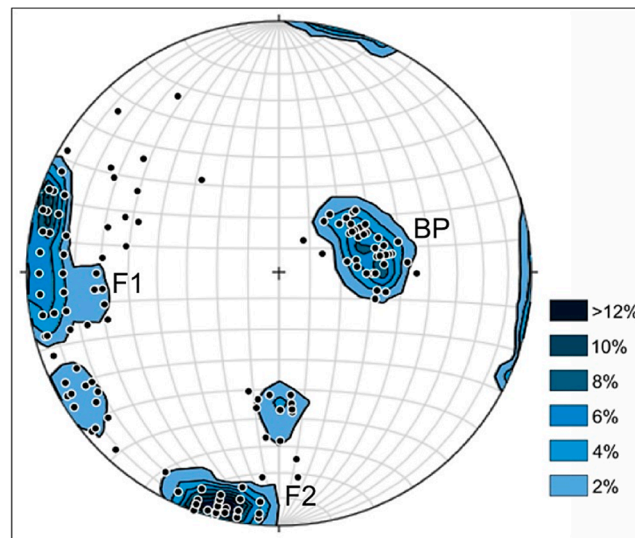


Figure 2. Equal-area projection of discontinuity poles measured in three outcrops (contour interval = 2%) showing the bedding plane (BP) and two fracture sets (F1 and F2).

Table 1. Characteristics of the three distinguished discontinuity sets, bedding plane (BP) and two sub-vertical fracture sets (F1 and F2).

Characteristic	Statistics	Set 1: BP	Set 2: F1	Set 3: F2
Orientation	Number of measurements	48	96	68
	Mean dip direction (°)	255.1	91.9	11.9
	Mean dip angle (°)	29.2	78.1	75.8
	Fisher dispersion coefficient	68.7	13.0	21.6
Spacing	Number of measurements	64	74	133
	Mean (cm)	26.20	24.45	10.47
	Standard deviation (cm)	1.77	2.01	1.38
Aperture	Number of measurements	97	187	161
	Mean aperture (mm)	0.12	0.15	0.15
	Standard deviation (mm)	0.19	0.26	0.21

A simplified model of the fracture network has been considered for a first estimate of the hydraulic properties of the rock mass.

If the fractured rock mass is assumed to have an impermeable matrix, if the discontinuities are considered as parallel plate model, with an aperture a and a spacing d , and if the groundwater moves by laminar flow in the discontinuities, the hydraulic conductivity k_i of each set can be estimated according to the cubic law [34]:

$$k_i = \frac{a^3 g}{12\nu d} \tag{1}$$

where g is the gravitational acceleration and ν is the kinematic viscosity of water.

The values of a and d introduced in Equation (1) are the mean values of the apparent aperture and spacing resulting from the statistical analysis (Table 1). The calculated hydraulic conductivities of the different sets ranged from 5×10^{-6} to 3×10^{-5} m/s (Table 2).

Table 2. Estimated hydraulic conductivity of each discontinuity set, bedding plane (BP) and two sub-vertical fracture sets (F1 and F2).

Set	k (m/s $\times 10^{-5}$)
Set 1: BP	0.54
Set 2: F1	1.13
Set 3: F2	2.64

If the discontinuities are well-connected and if the flows between the discontinuity sets do not interfere, the hydraulic conductivity tensor of the fractured rock mass $[K]$ can be calculated based on the orientation of the discontinuity sets [35]:

$$[K] = \sum_{i=1}^n k_i \times H_{jl}^i, j, l = x, y, z$$

$$H_{jl}^i = [I - n^T \times n]$$
(2)

where k_i is the hydraulic conductivity of the i th-discontinuity set; I is the unit matrix; and n is the direction cosine vector whose components are expressed in terms of the dip azimuth and dip angle of the discontinuity set (with the following coordinate system: y -axis oriented north, x -axis oriented east and z -axis oriented along the vertical).

The principal axes of anisotropy and the diagonal components of $[K]$ in these directions were determined using the eigenvalues and eigenvectors of the matrix $[K]$. The eigenvalues and the orientation of the principal axes of the tensor are listed in Table 3.

Table 3. Values and orientation of the major, intermediate and minor components of the hydraulic conductivity of rock mass.

Components	Value (m/s $\times 10^{-5}$)	Trend ($^\circ$)	Plunge ($^\circ$)
Minor	1.58	201	15
Intermediate	3.19	109	6
Major	3.84	359	74

4.2. Injection Tests

The injection tests processing first included a study of the relation between the flow rate (q) and the net injection pressure (H_0). In some cases, the relations highlighted the opening and erosion processes in the discontinuities, while, in other cases, the void filling and essential laminar flow were noted.

The hydraulic conductivity k_L in each test interval was calculated by applying the following equation [36]:

$$k_L = \frac{q}{lH_0} \left[\frac{1}{2\pi} \left(1 + \ln \frac{l}{2r} \right) \right]$$
(3)

where l and r are the length of the injection section and the borehole radius, respectively; and q and H_0 are the flow rate and the net injection pressure values under laminar flow, respectively.

The calculated values of k_L fell within three orders of magnitude (10^{-8} – 10^{-6} m/s), with a geometric mean of 2.81×10^{-7} m/s. Figure 3 shows the k_L values of each borehole plotted *versus* the average depth of the injection section. At depths greater than 25 m, there was a significant decrease in the hydraulic conductivity, with the exception of the inclined borehole (LT8 in Figure 3). Above a depth of 25 m, the boreholes that were located in the valley bottom (LT4–LT8 in Figure 3), corresponding to a faulted zone, exhibited a higher k_L .

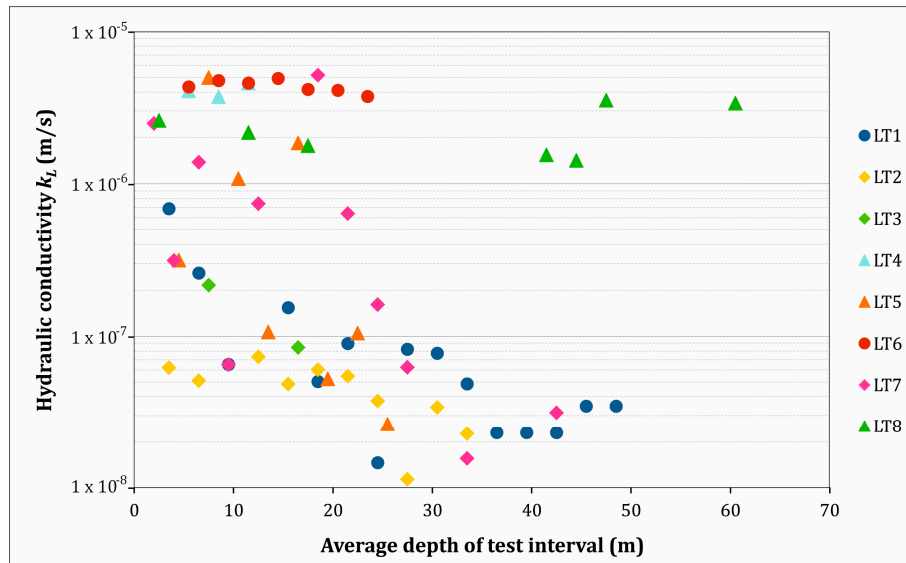


Figure 3. Hydraulic conductivity k_L from the injection tests *versus* the average depth of the injection section.

4.3. Pumping Tests

The pumping test data diagnosis included a comparison of the drawdown plots of each piezometer with theoretical models to determine the aquifer parameters. This analysis showed that the Theis [37], leaky aquifer [38] and double porosity [39] models could explain most of the measured drawdowns; in some cases, two or three theoretical models interpreted the same drawdown-time trend without significant differences in the calculated aquifer parameters, *i.e.*, the transmissivity and storage coefficient. For wells with more than one piezometer, there was a simultaneous response in the pumping, and generally, a similar shape for the drawdown curve for the different observation wells was reported, as observed in Figure 4.

Table 4 summarizes the results of the aquifer parameters, which were calculated as an average value when more than one model presented a good fit with the measured data and with the statistics of the curve matching. The overall transmissivity and storage coefficients varied from 2.3×10^{-4} to 3.6×10^{-3} m²/s and from 3.1×10^{-5} to 2.6×10^{-2} , respectively. The transmissivities were converted into hydraulic conductivities (K_P) based on the saturated aquifer thickness intercepted by the tested well. The values of K_P fell in the range of 4.6×10^{-6} – 4.1×10^{-5} m/s, with a geometric mean of 1.68×10^{-5} m/s.

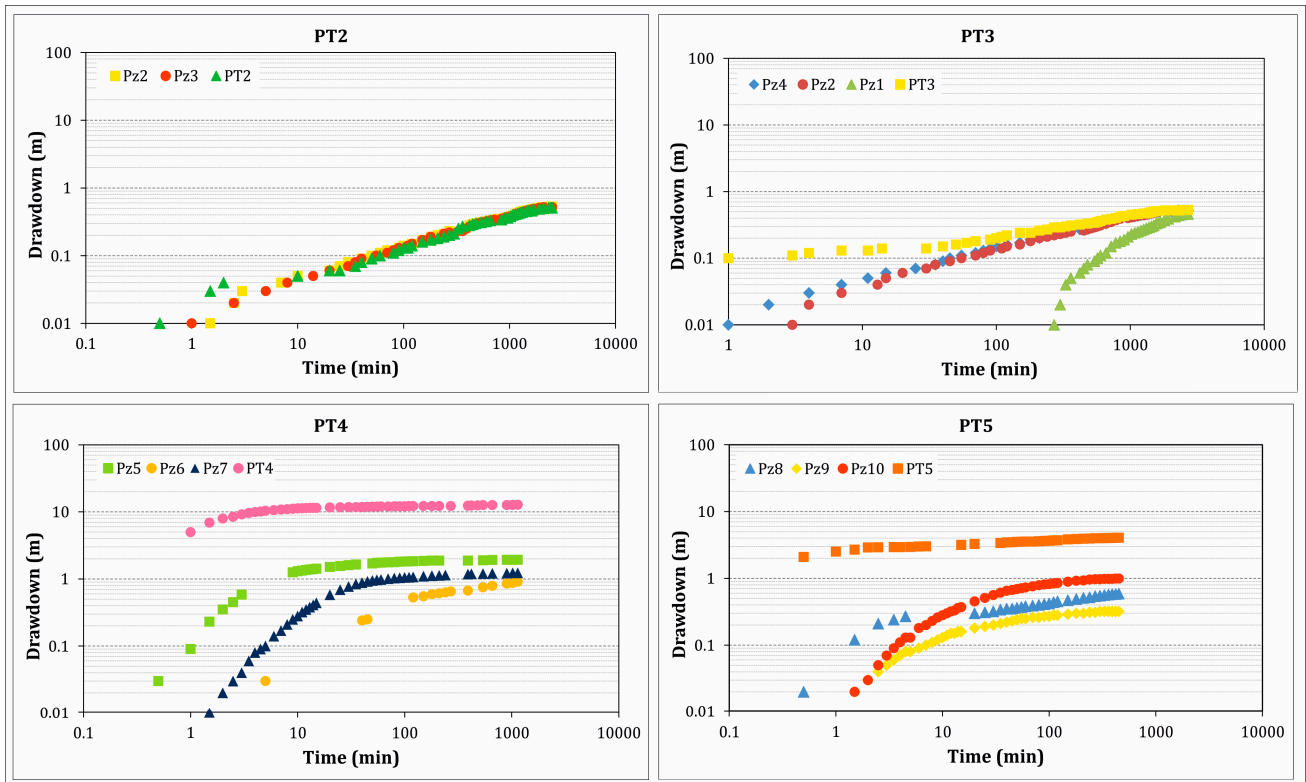


Figure 4. Drawdown-time plots resulting from the pumping tests for the wells with more observation piezometers.

Table 4. Results of the pumping tests: Q , constant rate of pumping; H_{sat} , saturated thickness of the aquifer intercepted by the well; T , transmissivity; K_P , hydraulic conductivity; S , storage coefficient; RSS, sum of squared residuals.

Well	Q (m ³ /s)	H_{sat} (m)	Piezometer	T (m ² /s)	K_P (m/s)	S	RSS
PT1	2.1×10^{-3}	50	Pz1	4.89×10^{-4}	9.78×10^{-6}	2.61×10^{-2}	0.001
PT2	2.3×10^{-3}	41	Pz2	1.44×10^{-3}	3.51×10^{-5}	1.85×10^{-3}	0.024
			Pz3	1.42×10^{-3}	3.46×10^{-5}	5.11×10^{-3}	0.024
PT3	2.4×10^{-3}	53	Pz4	1.51×10^{-3}	2.85×10^{-5}	7.29×10^{-3}	0.021
			Pz2	1.41×10^{-3}	2.66×10^{-5}	4.56×10^{-3}	0.023
			Pz1	4.46×10^{-4}	8.41×10^{-6}	1.80×10^{-2}	0.002
PT4	2.5×10^{-3}	50	Pz5	2.32×10^{-4}	4.64×10^{-6}	3.15×10^{-5}	0.045
			Pz6	9.50×10^{-4}	1.90×10^{-5}	6.26×10^{-4}	0.013
			Pz7	2.33×10^{-4}	4.66×10^{-6}	5.22×10^{-4}	0.035
PT5	3.5×10^{-3}	86	Pz8	3.57×10^{-3}	4.15×10^{-5}	9.92×10^{-4}	0.023
			Pz9	3.44×10^{-3}	4.00×10^{-5}	8.83×10^{-4}	0.001
			Pz10	8.24×10^{-4}	9.58×10^{-6}	2.64×10^{-4}	0.002

4.4. Groundwater Flow Model

The hydrogeological characterization of the site was completed by a potentiometric surface reconstruction over the entire dam site using the head data measured in 70 wells and boreholes during the initial reservoir filling when the artificial lake level was at 121 m a.s.l. [30]. The head contour line

deformation due to the lake and due to the gaining river was obtained by adding head points along the boundary conditions; the dam effect (*i.e.*, the upstream impervious face and grout curtain) was obtained by applying an impervious bound in the Kriging interpolation technique. From Figure 5, where the head distribution and the standard error ranges associated with the Kriging prediction are shown, it appears that the head contour lines generally replicate the topography. On the left of the dam, the lake feeds groundwater which discharges into River Pittiu and laterally bypasses the grout curtain flowing towards the rockfill embankment of the dam.

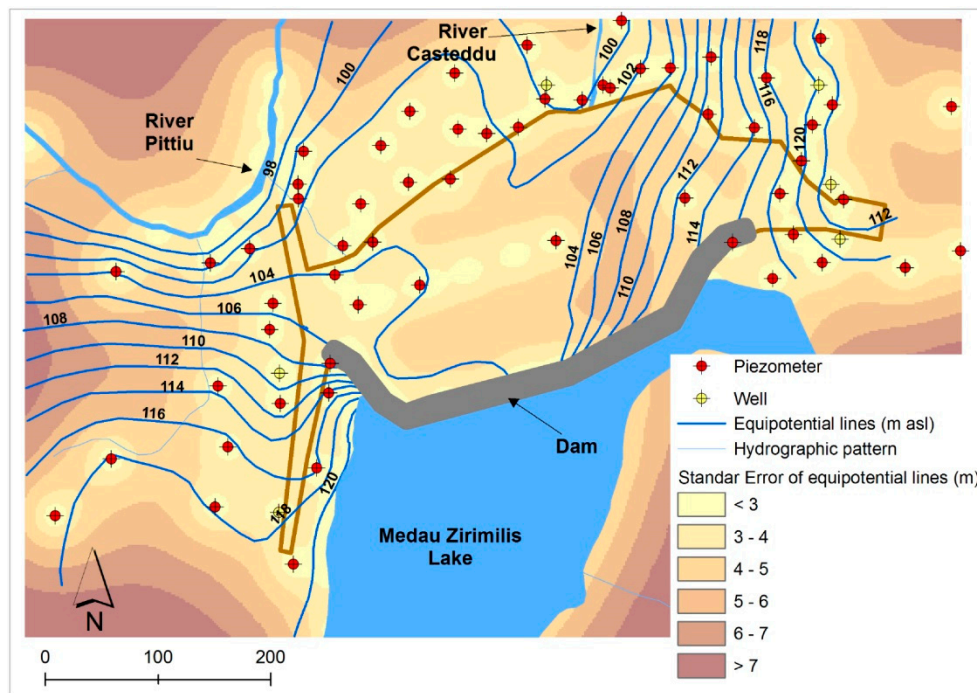


Figure 5. Potentiometric map at the site of the Medau Zirimilis Dam reconstructed by the kriging interpolation technique and the associated ranges of standard error when the artificial lake level was at 121 m a.s.l.

Thanks to the presence of physical boundary conditions (lake and river) and to the presence of both pumping tests and surface fracture survey, the western sector of the dam was selected for the numerical simulation (Figure 1).

The model involved an area of 86,750 m² (Figure 6). The grid consisted of one layer of 8736 cells with a telescopic refinement around the pumping well (PT4) and side dimensions from 0.33 to 8 m. As the investigations revealed, the bottom of the aquifer was not well defined; the available stratigraphic logs were compared with the results of injection and pumping tests and the model bottom was set at a depth of 50 m from ground surface. The aquifer was considered continuous, unconfined and isotropic, as resulted from field investigations.

The boundary conditions included: constant head boundary for the lake (*i.e.*, water level at 121 m a.s.l.); drain boundary condition for the gaining stream (*i.e.*, River Pittiu) and for section of the dam embankment where flow was measured in the drainage systems; no-flow cells in sectors outside the domain of interest or along groundwater divides (western side); well boundary condition for the pumping well (*i.e.*, PT4 well); constant flux boundary condition for the southern boundary (Figure 6).

No precipitation event occurred in the days before and during the pumping tests, therefore no areal recharge was applied.

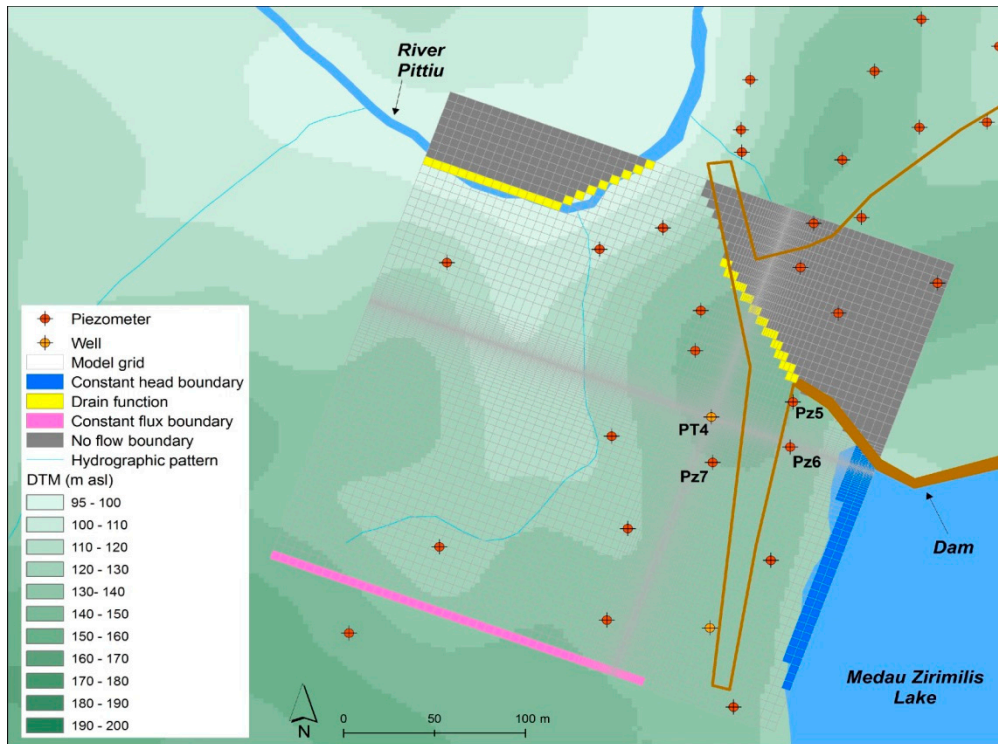


Figure 6. Grids and boundary conditions of the numerical model. DTM: digital terrain model.

The days in which the pumping test was performed, a constant pumping rate of $2.5 \times 10^{-3} \text{ m}^3/\text{s}$ from the well PT4 was measured. The same day the lake level was 121 m a.s.l. and a flow of $6.7 \times 10^{-3} \text{ m}^3/\text{s}$ was measured from the horizontal drain located at the base of the embankment in the left sector of the dam [30]. If we consider the portion of the drain that falls within the modeled area, a maximum outflow of $3 \times 10^{-3} \text{ m}^3/\text{s}$ is expected from this model boundary. Outflow from River Pittiu was not measured during the days of the test.

Inflows from the southern and lake boundaries were estimated. For the southern boundary, considering the surface area of the upstream potential groundwater basin drained from this section, an area of about 2 km^2 is obtained. Base flow measures are available for an instrumented basin which is morphologically and geologically comparable with the basin under investigation, resulting between 2×10^{-3} and $4 \times 10^{-3} \text{ m}^3/\text{s}$ per km^2 (*i.e.*, River Fluminimaggiore; [40]). According to this information, an inflow from 4×10^{-3} to $8 \times 10^{-3} \text{ m}^3/\text{s}$ is expected from the southern boundary. A second estimate considers the hydraulic gradient and transmissivity of this sector of the dam site and the length of boundary, obtaining an inflow ranging between 5×10^{-3} and $6 \times 10^{-3} \text{ m}^3/\text{s}$. Using this last approach for the lake boundary, an inflow ranging between 4×10^{-3} and $5 \times 10^{-3} \text{ m}^3/\text{s}$ results.

The model underwent an initial calibration through the trial-and-error technique. The main purposes of this step were to test the numerical stability of the model and to roughly reduce the initial difference between the observed and calculated values of the observation points. This step preceded the application of the parameter estimation code PEST 13.0 [41], which was applied in two different modes: classical zone calibration and pilot point calibration [42,43].

A steady-state calibration was used as the first time period of the transient simulation. A second time period, divided into 20 steps, was introduced with pumping from PT4 at a constant rate ($2.5 \times 10^{-3} \text{ m}^3/\text{s}$) for 19 hours. Transient data were calibrated for the pumping well (PT4) and Pz5 and Pz7 piezometers.

A sensitivity analysis of the transient model highlighted the significant influence of the bottom elevation, which was only known in coincidence of boreholes and piezometers. Therefore the results were expressed by translating the hydraulic conductivity into transmissivity.

In Figure 7, simulated contour lines at the end of 19 h and transmissivity distribution are reported. In the same figure the simulated and observed heads of all wells and piezometers are shown, as well as the trends of drawdown in the PT4 well and in the Pz5 and Pz7 piezometers. The calibrated values of the specific yield are within the order of magnitude of 10^{-4} . The water balance is shown in Table 5 in comparison with measurements and analytical computations of the flows.

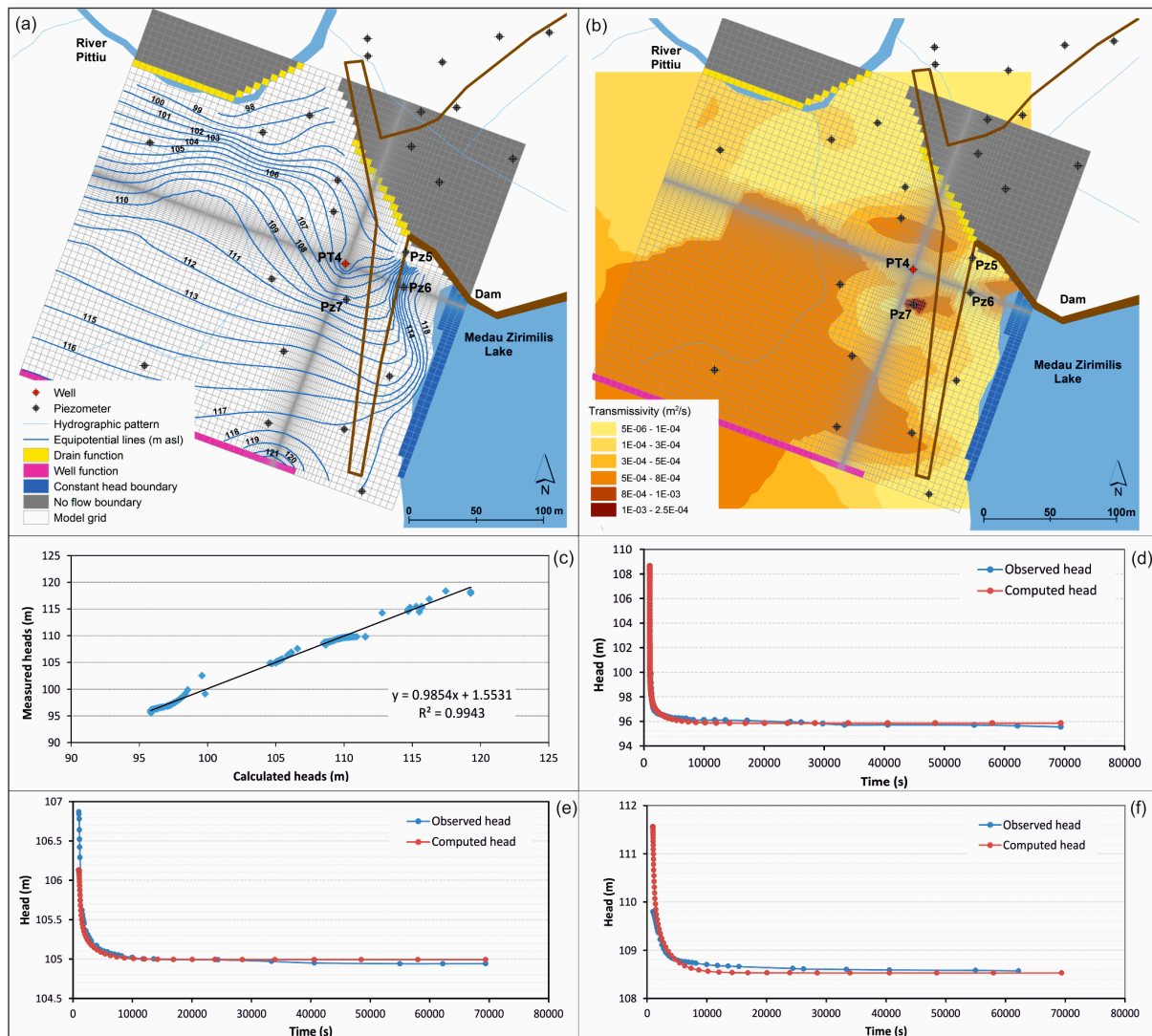


Figure 7. Results of the transient-state calibrated model showing (a) the potentiometric contour map; (b) the transmissivity distribution; (c) the scatter plot of the measured and calculated heads; (d) the comparison of the observed and calculated heads for the PT4 tested well; (e) for the Pz5 piezometer and (f) for the Pz7 piezometer.

Table 5. Groundwater budget resulting from the numerical model compared with the estimated terms from the conceptual model.

Model	Inflow ($\times 10^{-3} \text{ m}^3/\text{s}$)				Outflow ($\times 10^{-3} \text{ m}^3/\text{s}$)		% Error (in-out)
	Lateral Boundaries	Lake	Storage	Well	River	Lateral Boundaries	
Numerical Model	6.84	3.10	0.08	2.50	5.69	1.81	0.2
Conceptual model	4–8	4–5	-	2.50	na	3	-

Notes: na: not available.

Composite sensitivities associated with pilot points were calculated for the transient model with reference to the hydraulic conductivity, *i.e.*, the parameter that mainly affects the results. Highest values of composite sensitivity are associated to the pilot points corresponding with the pumping well PT4 and those falling in its surroundings (Figure 8), where the highest number of observations is located. Therefore, we can assume a good representativeness of the calibrated hydraulic conductivity in this zone, where the calibrated parameters give ranges of transmissivity from 5.0×10^{-6} to $2.5 \times 10^{-3} \text{ m}^2/\text{s}$.

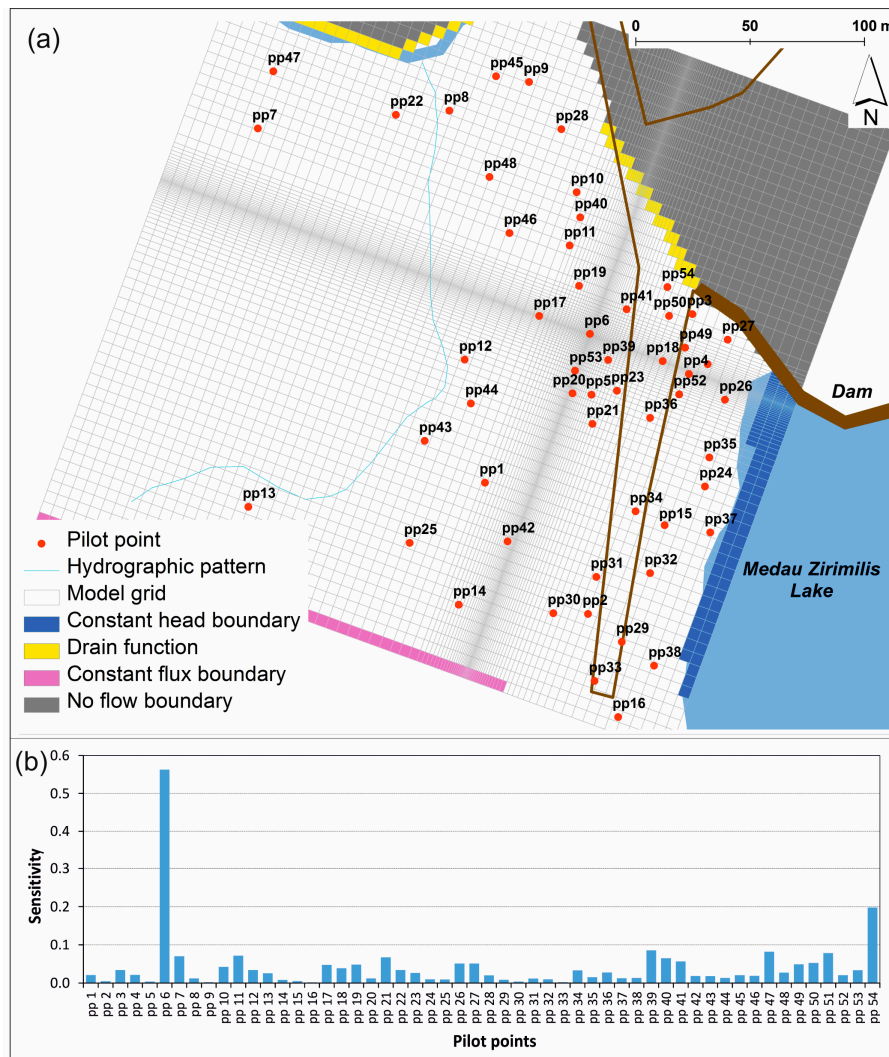


Figure 8. (a) Distribution of the pilot points in the model domain and (b) values of composite sensitivities for each point.

5. Discussion

Investigations concerning fractured metamorphic rocks in a representative area of Sardinia can be used to hydrogeologically characterize these low-permeability rocks and to examine which approach can be used to represent the fractured aquifer. By interfacing the results of surface fracture surveys, injection tests and pumping tests with those of a flow numerical model, we inspected if the porous equivalent approach could (or could not) provide a good approximation of a fractured aquifer.

The surface fracture survey provides a model of rock mass that is characterized by a well-developed discontinuity network (three discontinuity sets), a high frequency of discontinuities (spacing of less than 0.5 m) and comparable values of the average apparent aperture of the different sets (approximately 0.1 mm). Therefore the results of the surface fracture survey implied the possibility of considering the fractured medium as an equivalent porous medium at the outcrop scale, because the discontinuity network gives rise to a reduced representative elementary volume (less than 1 m³) for the rock mass.

The discontinuity network produces a slight anisotropy in the medium, with the major principal component of the hydraulic conductivity directed vertically downward, as expected given the predominance of vertical discontinuities over horizontal ones in the studied area. However, the modules of the hydraulic conductivity determined for the rock mass should be considered in relative terms and not in absolute terms because the apparent aperture does not correspond to the hydraulic aperture. A greater reliability can be assigned to the orientation of the three principal components, independent from the aperture.

The injection tests clearly showed the extreme heterogeneity of the rock mass, as highlighted by the wide range of values determined for the hydraulic conductivity (10⁻⁸–10⁻⁶ m/s). This can be interpreted by considering the variability of the rock mass fracturing in relation to the proximity to the faulted zone in the valley of the dam site. The highest values of hydraulic conductivity were found for the inclined borehole, which was close to the fault zone and, thus, intercepted a great number of vertical fractures. With the exception of the inclined borehole close to fault zone, the hydraulic conductivity was observed to diminish below a depth of 25 m.

The hydraulic conductivity derived from the pumping tests covered a lower range of values (10⁻⁶–10⁻⁵ m/s) than did those calculated using the injection tests. No particular trend was evident from the comparison of the values of hydraulic conductivity obtained for piezometers located in different directions from the pumped well. The variation in the parameter is therefore attributable to the heterogeneity of the aquifer rather than to its horizontal anisotropy. Moreover, if we consider the simultaneous response to pumping and the similar shape of the drawdown curves for the different piezometers when the pumping was performed from the same well, the porous medium approximation appears appropriate.

The comparison between the hydraulic conductivity determined by the injection tests and the pumping tests revealed values that were substantially lower in the first case (Figure 9). This can be attributed to the limited volume of rock mass affected by the injection tests compared to that affected by the pumping tests. In both cases, the hydraulic heterogeneity of the rock mass was evident. The injection tests and the pumping tests also converged and indicated higher hydraulic conductivities near the fault that runs in the valley of the dam site (Figure 3 and Table 4). Instead, the limit for the

determination of the aperture by the surface survey did not permit a direct comparison of the hydraulic conductivity values determined using this method. However, if the average hydraulic conductivity (*i.e.*, the geometric mean) calculated from the pumping tests and the average spacing of the three sets determined from the surface survey are introduced in Equation (1), the average aperture value would be 0.16 mm, which is comparable with those measured in outcrop. However, the range of hydraulic conductivity resulting from the surface survey (10^{-6} – 10^{-5} m/s) is consistent with that evaluated by pumping tests (Figure 9).

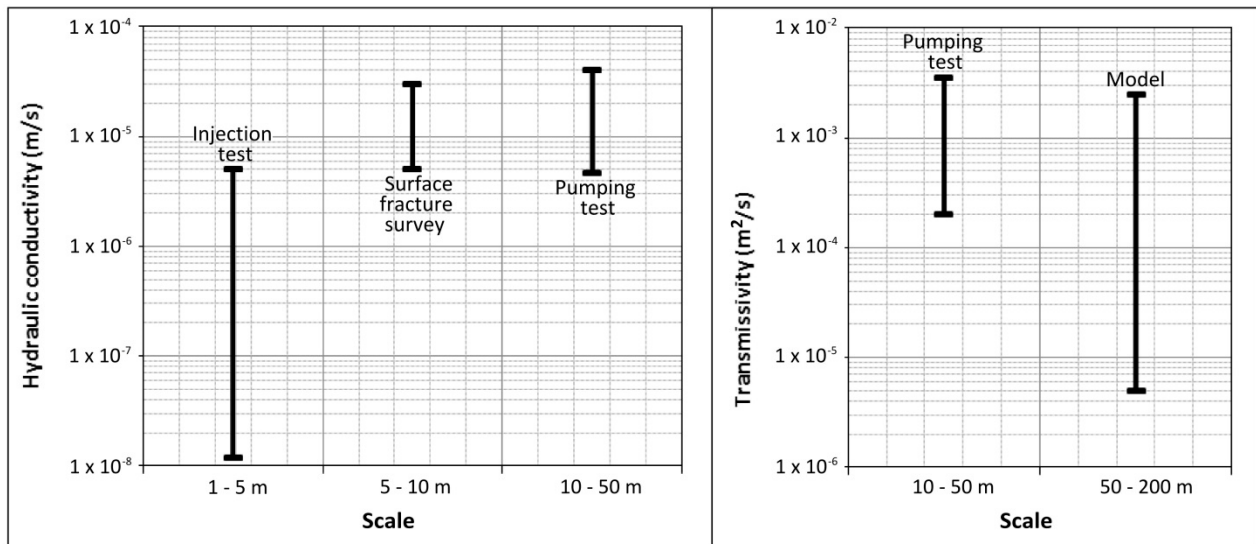


Figure 9. Hydraulic parameters and scale of measurement of the different methods used.

This scale effect of the parameter is expected in heterogeneous media [44–47] because the volume investigated by the injection tests was significantly smaller than that of the pumping tests. In the graph of Figure 9 one can see that the range of hydraulic conductivity values obtained from the surface fracture survey is consistent with the increase of hydraulic conductivity with the increase of the measuring scale. This implies that the results of surface fracture survey can be considered in the characterization of hard rocks when the discontinuity apertures are measured on the unweathered portions of discontinuity, at least to identify the order of magnitude of the parameter.

The numerical model considered one representative pumping test and provided additional information on the hydrogeological characterization of the hard rocks.

The results of the field investigations together with the model output would encourage the equivalent porous approach, at least in geological situations similar to that here considered. The estimate of transmissivity resulting from the model highlighted a range of values higher than those resulting from the pumping tests. However, the transmissivity values determined in the pumping tests (from 10^{-4} to 10^{-3} m^2/s) fell in the range of the calibrated values of the model (from 10^{-6} to 10^{-3} m^2/s), with a common upper limit of the parameter (Figure 9). This still seems to be consistent with what is reported in the literature, *i.e.*, that the increase in average permeability apparently does not continue from the pumping test to a regional scale [44,45]. On the other hand, four orders of magnitude of transmissivity obtained from the model compared with two orders of magnitude from the pumping

tests, highlight a high hydraulic heterogeneity of the aquifer, this time in agreement with the results of the injection tests.

6. Conclusions

The multi-scale characterization of the metamorphic rocks of the area studied herein demonstrated that the continuum medium approach can be used when a dense network of discontinuities exists (representative elementary volume of few cubic meters), as in the case of the fractured aquifer examined. What strongly affects this approach is the hydraulic heterogeneity of the medium. The multi-scale approach is thus recommended for investigating the hydraulic heterogeneity, and it can help to manage uncertainty by placing greater trust in the obtained results. In particular, it is evident that the surface fracture survey enhances the hydraulic characterization of fractured rocks, when the fracturing affects the layers closest to the surface, as the general case of the hard-rock aquifers.

Regarding the transmissivity of the examined hard-rock aquifer, it falls in the classes III and IV of the classification proposed by Krasny [48], corresponding to rocks from low to intermediate transmissivity magnitude. This aquifer, commonly believed to be not productive, may be of interest for the local water supply, especially if one considers the large extent of these rocks and the scarcity of water resources in Sardinia. The same concept could be applied in other regions of the world where these aquifers outcrop over very large areas. In this regard, our findings confirm that the most promising areas for well location correspond to valleys close to faulted zones where transmissivity increases; in these specific zones a relative higher yield of wells is expected, especially in case of boreholes inclined according to an angle which can be determined after the fracture characterization.

Acknowledgments

The authors wish to thank the two anonymous reviewers for their constructive comments and suggestions. Vincenzo Piscopo want to remember recently deceased Pietro Celico to have introduced him with passion and dedication to hydrogeology.

Author Contributions

All of the authors contributed extensively to the work. Vincenzo Piscopo led the research. Antonella Baiocchi, Francesca Lotti and Simone Piacentini performed the data analysis and numerical modeling. Walter Dragoni contributed to the manuscript review. All authors contributed to the manuscript preparation, discussing and sharing the conclusions.

Conflicts of Interest

The authors declare no conflict of interest.

References

1. Banks, D.; Banks, S. Hydrogeology of Hard Rocks. In Proceedings of the Memoires of the 24th Congress, International Association of Hydrogeologists, Oslo, Norway, 28th June–2nd July 1993; volume 28, pp. 1–684.

2. Stober, I.; Bucher, K. *Hydrogeology of Crystalline Rocks*; Kluwer Academic Publishers: Dordrecht, The Netherlands, 2003.
3. Taylor, R.; Howard, K. A tectono-geomorphic model of the hydrogeology of deeply weathered crystalline rock: Evidence from Uganda. *Hydrogeol. J.* **2000**, *8*, 279–294.
4. Cho, M.; Ha, K.-M.; Choi, Y.-S.; Kee, W.-S.; Lachassagne, P.; Wyns, R. Relationship between the Permeability of Hard-Rock Aquifers and Their Weathered Cover Based on Geological and Hydrogeological Observation in South Korea. In Proceedings of the IAH Conference on “Groundwater in fractured rocks”, Prague, Czech, 15–19 September 2003.
5. Dewandel, B.; Lachassagne, P.; Wyns, R.; Maréchal, J.C.; Krishnamurthy, N.S. A generalized 3-D geological and hydrogeological conceptual model of granite aquifers controller by single or multiphase weathering. *J. Hydrol.* **2006**, *320*, 260–284.
6. Krasny, J.; Sharp, J.M. *Groundwater in Fractured Rocks*; Taylor & Francis: London, UK, 2007.
7. Foster, S. Hard-rock aquifers in tropical regions: Using science to inform development and management policy. *Hydrogeol. J.* **2012**, *20*, 659–672.
8. Sharp, J.M. *Fractured Rock Hydrogeology*; Taylor & Francis: London, UK, 2014.
9. Uhl, V.W.; Sharma, G.K. Results of pumping tests in crystalline-rock aquifers. *Ground Water* **1978**, *16*, 192–203.
10. Howard, K.W.K.; Hughes, M.; Charlesworth, D.L.; Ngobi, G. Hydrogeologic evaluation of fracture permeability in crystalline basement aquifers of Uganda. *Hydrogeol. J.* **1992**, *1*, 55–65.
11. Chilton, P.J.; Foster, S.S.D. Hydrogeological characteristics and water-supply potential of basement aquifers in tropical Africa. *Hydrogeol. J.* **1995**, *3*, 3–49.
12. Maréchal, J.C.; Dewandel, B.; Subrahmanyam, K. Use of hydraulic tests at different scales to characterize fracture network properties in the weathered-fractured layer of a hard rock aquifer. *Water Resour. Res.* **2004**, *40*, doi:10.1029/2004WR003137.
13. Banks, D.; Gundersen, P.; Gustafson, G.; Makela, J.; Morland, G. Regional similarities in the distributions of well yield from crystalline rocks in Fennoscandia. *Norges Geol. Unders. Bull.* **2010**, *450*, 33–47.
14. Lee, C.H.; Chang, J.L.; Deng, B.W. A continuum approach for estimating permeability in naturally fractured rocks. *Eng. Geol.* **1995**, *39*, 71–85.
15. Scanlon, B.R.; Mace, R.E.; Barrett, M.E.; Smith, B. Can we simulate regional groundwater flow in a karst system using equivalent porous media models? Case study, Barton Springs Edwards aquifer, USA. *J. Hydrol.* **2003**, *276*, 135–158.
16. Lemieux, J.-M.; Therrien, R.; Kirkwood, D. Small scale study of groundwater flow in a fractured carbonate-rock aquifer at the St-Eustache quarry, Québec, Canada. *Hydrogeol. J.* **2006**, *14*, 603–612.
17. Long, J.C.S.; Remer, J.S.; Wilson, C.R.; Witherspoon, P.A. Porous media equivalents for networks of discontinuous fractures. *Water Resour. Res.* **1982**, *18*, 645–658.
18. Hsieh, P.A.; Neuman, S.P.; Stiles, G.K.; Simpson, E.S. Field determination of the three-dimensional hydraulic conductivity tensor of anisotropic media. 2 Methodology and application to fractured rocks. *Water Resour. Res.* **1985**, *21*, 1667–1676.
19. Neuman, S.P. Stochastic Continuum Representation of Fractured Rock Permeability as an Alternative to the Rev and Fracture Network Concepts. In Proceedings of the 28th US Symposium on Rock Mechanics, Tucson, AZ, USA, 29 June–1 July 1987; pp. 533–561.

20. Bradbury, K.R.; Muldoon, M.A.; Zapotec, A.; Levy, J. *Delineation of Wellhead Protection Areas in Fractured Rocks*; US EPA Technical Guidance Document, EPA 570/9-91-009; EPA: Washington, DC, USA, 1991.
21. Nuclear Regulatory Commission (NRC). *Rock Fractures and Fluid Flow: Contemporary Understanding and Applications*; National Academy Press: Washington, DC, USA, 1996.
22. Neuman, S.P. Trends, prospects and challenge in quantifying flow and transport through fractured aquifer. *Hydrogeol. J.* **2005**, *13*, 124–147.
23. Baiocchi, A.; Dragoni, W.; Lotti, F.; Piscopo, V. Sustainable yield of fractured rock aquifers: The case of crystalline rocks of Serre Massif (Calabria, Southern Italy). In *Fractured Rock Hydrogeology*; Sharp, J.M., Ed.; Taylor & Francis Group: London, UK, 2014; pp. 79–97.
24. Dragoni, W. Some considerations on climatic changes, water resources and water needs in the Italian region south of the 43° N. In *Water, Environment and Society in Times of Climatic Change*; Issar, A., Brown, N., Eds.; Kluwer Academic Publishers: Dordrecht, The Netherlands, 1998; pp. 241–271.
25. Intergovernmental Panel on Climate Change (IPCC). Summary for Policymakers. In *Climate Change 2013: The Physical Science Basis*; Cambridge University Press: Cambridge, UK, 2013.
26. Carmignani, L.; Coccozza, T.; Gandin, A.; Pertusati, P.C. Lineamenti della geologia dell'Iglesiente-Sulcis [Outlines of the geology of the Iglesias-Sulcis Region]. In *Guida alla Geologia del Paleozoico Sardo*; Società Geologica Italiana, Guide Geologiche Regionali: Roma, Italy, 1982; pp. 65–77.
27. Istituto Superiore per la Protezione e la Ricerca Ambientale (ISPRA). *Notes to the Geological Map of Italy 1:50,000 "Sheet 566-Assemini"*; Servizio Geologico d'Italia: Roma, Italy, 2009. (In Italy)
28. Barca, S.; Coccozza, T.; del Rio, M.; Pittau Demelia, P. Discovery of lower Ordovician Acritarchs in the "Postgotlandiano" sequence of southwestern Sardinia (Italy): Age and tectonic implications. *Boll. Soc. Geol. Ital.* **1981**, *100*, 377–392.
29. Carmignani, L.; Conti, P.; Barca, S.; Cerbai, N.; Eltrudis, A.; Funedda, A.; Oggiano, G.; Patta, E.D. *Notes to the Geological Map of Italy 1:50,000 "Sheet 549-Muravera"*; Servizio Geologico d'Italia: Roma, Italy, 2001. (In Italy)
30. Celico, P.; Piscopo, V.; Berretta, G. Influence of a reservoir on groundwater flow in metamorphic rocks. *Geol. Appl. Idrogeol.* **1993**, *28*, 253–261. (In Italy)
31. Kruseman, G.P.; de Ridder, N.A. *Analysis and Evaluation of Pumping Test Data*; ILRI Publication 47; International Institute for Land Reclamation and Improvement: Wageningen, The Netherlands, 1994.
32. Allmendinger, R.W.; Cardozo, N.C.; Fisher, D. *Structural Geology Algorithms: Vectors & Tensors*; Cambridge University Press: Cambridge, UK, 2013.
33. Cardozo, N.; Allmendinger, R.W. Spherical projections with OSX Stereonet. *Comput. Geosci.* **2013**, *51*, 193–205.
34. Snow, D.T. Anisotropic permeability of fractured media. *Water Resour. Res.* **1969**, *5*, 1273–1289.
35. Oda, M. Permeability tensor for discontinuous rock masses. *Geotechnique* **1985**, *35*, 483–495.
36. Moye, D.G. Diamond drilling for foundation exploration. *Civil Eng. Trans. Inst. Eng.* **1967**, *9*, 95–100.

37. Theis, C.V. The relation between the lowering of the piezometric surface and the rate and duration of discharge of a well using groundwater storage. *Am. Geophys. Union Trans.* **1935**, *2*, 519–524.
38. Hantush, S.M.; Jacob, C.E. Non-steady radial flow in an infinite leaky aquifer. *Am. Geophys. Union Trans.* **1955**, *36*, 95–100.
39. Warren, J.E.; Root, P.J. The behavior of naturally fractured reservoirs. *One Petro* **1963**, *3*, 245–255.
40. Regione Sardegna (2010) Annali Idrologici. Available online: www.regione.sardegna.it (accessed on 25 October 2014).
41. Doherty, J. *PEST, Model-Independent Parameter Estimation—User Manual*, 5th ed.; Watermark Numerical Computing: Brisbane, Australia, 2010.
42. De Marsily, G.; Lavedan, C.; Boucher, M.; Fasaniso, G. Interpretation of interference tests in a well field using geostatistical techniques to fit the permeability distribution in a reservoir model. In *Geostatistics for Natural Resources Characterization*; NATO Advanced Study Institute: Dordrecht, The Netherlands, 1984; pp. 831–849.
43. Doherty, J. Groundwater model calibration using pilot-points and regularization. *Ground Water* **2003**, *41*, 170–177.
44. Clauser, C. Permeability of crystalline rocks. *EOS* **1992**, *73*, 233–240.
45. Schulze-Makuch, D.; Carlson, D.A.; Cherkauer, D.S.; Malik, P. Scale dependency of hydraulic conductivity in heterogeneous media. *Ground Water* **1999**, *37*, 904–919.
46. Renard, P.; de Marsily, G. Calculating equivalent permeability: A review. *Adv. Water Res.* **1997**, *20*, 253–278.
47. Neuman, S.P.; di Federico, V. Multifaceted nature of hydrogeologic scaling and its interpretation. *Rev. Geophys.* **2003**, *41*, doi:10.1029/2003RG000130.
48. Krasny, J. Classification of transmissivity magnitude and variation. *Ground Water* **1993**, *31*, 230–236.

© 2015 by the authors; licensee MDPI, Basel, Switzerland. This article is an open access article distributed under the terms and conditions of the Creative Commons Attribution license (<http://creativecommons.org/licenses/by/4.0/>).